Toxicity of Curcumin Nanoparticles towards Alveolar Macrophage: Effects of Surface Charges

Ching-Yee Loo[1], Ee Ling Siew[2,3], Paul M. Young[4, 5], Daniela Traini[4,6] and Wing-Hin Lee[1 *]

[1]Faculty of Pharmacy and Health Sciences, Royal College of Medicine Perak, Universiti Kuala Lumpur (UniKL RCMP), 30450 Perak, Malaysia

[2]Asasipintar UKM Program, Pusat Genius@Pintar Negara, Universiti Kebangsaan Malaysia 43600 Bangi, Selangor, Malaysia

[3]Biocompatibility and Toxicology Laboratory, Centre for Research and Instrumentation Management (CRIM), Universiti Kebangsaan Malaysia, 43600 Bangi, Malaysia

[4] Respiratory Technology, Woolcock Institute of Medical Research, Sydney, NSW 2037 Australia

[5]Department of Marketing, Macquarie Business School, Macquarie University, NSW 2109, Australia

[6]Department of Biomedical Sciences, Faculty of Medicine, Health and Human Sciences Macquarie University, NSW 2109, Australia

*Corresponding author
Wing-Hin Lee
Faculty of Pharmacy and Health Sciences,
Royal College of Medicine Perak, Universiti Kuala Lumpur (UniKL RCMP), Ipoh, Perak, Malaysia
Email: whlee@unikl.edu.my
Tel: +605-243 2365 ext 852
Fax: +605-243 2636

Keywords: alveolar macrophage; curcumin; nanoparticle; toxicity; surface charge

Abstract

Curcumin has been used for chronic lung diseases management due to its diversified molecular actions. However, the potential cytotoxicity which occurs in cells following the exposure to high concentrations of curcumin has been overlooked. This study evaluated the toxic events of curcumin nanoparticles (Cur-NPs) with alterable surface polarity in alveolar macrophages (NR8383). We aimed to establish the correlation between the toxicity of Cur-NPs with different surface charges and the internalization mechanisms of the NPs. Toxicity data showed that positively charged Cur-NPs (IC_{50}: 9.77±0.5 µg/mL) was the most potent against NR8383, followed by negatively charged Cur-NPs (IC_{50}:13.33±0.9 µg/mL) and neutral Cur-NPs (IC_{50}:18.68±1.2 µg/mL). Results from mitochondrial membrane potential, ATP content and intracellular ROS in NR8383 showed similar ranking to the toxicity assay. The predominant uptake pathway for positively and negatively charged Cur-NPs was via clathrin-mediated endocytosis, while neutral Cur-NPs was internalized via phagocytosis, micropinocytosis and clathrin-mediated endocytosis. Positively charged Cur-NPs mediates the cytotoxicity of NR8383 via lysosomal and mitochondrial-associated destabilization upon entry. In conclusion, the cytotoxicity of Cur-NPs on NR8383 is surface-charge dependent, which in turn is associated to the uptake pathway and localization of Cur-NPs in cells.

1. Introduction

The inhalation of toxic substances (i.e., cigarette smoke, toxic gas), continuous exposure to fine particulate matter (i.e., dust), allergen and air-borne microorganisms contributes to abnormal inflammatory and oxidative-stress related responses, as well as adaptive immune response in the lung (Laskin et al., 2019; Lugg et al., 2021). The overproduction of reactive oxygen species (ROS) is one of the contributing factors facilitating DNA damage, lipid peroxidation, inflammation and activating-oncogenes related pathways leading to lung disease progression (Aggarwal et al., 2019; Zhang et al., 2014). It is established that the pulmonary immune system is mediated by alveolar macrophages as response to invasion of foreign particles. The invasion of pulmonary toxicants/particles is first engulfed by resident alveolar macrophages and rapidly cleared from the lung, either through the mucociliary escalator or proximal lymph nodes (2005). Simultaneously, these alveolar macrophages orchestrate an immunological process by generating increasing levels of cytotoxic, pro-inflammatory mediators and extracellular ROS. However, the alveolar macrophage that overstayed in the lung contributed directly to the pathogenesis of lung diseases (Murthy et al., 2015).

Naturally occurring polyphenols are produced as secondary metabolites in plants with proven protective functions against oxidative-stress related injury, radiation damages and pathogen invasion (Abdel-Diam et al., 2019). Polyphenols are also effective to fight various chronic diseases like cancer, diabetes, cardiovascular and lung diseases (i.e., asthma, obstructive pulmonary disease (COPD) and lung cancer) (Lee et al., 2013). Curcumin, a polyphenol compound derived from turmeric, is popular for its pleotropic biological activities as evidenced by the large number of publications (*in vitro*, *in vivo* and human trials) for diverse diseases (Doello et al., 2018). The

application of curcumin, both as therapeutic and/or preventive agent, is hampered due to minimal solubility and stability in physiological conditions as well as its limited cellular internalization. As the maximal solubility of curcumin in aqueous solution is approximately 30 nM, it is necessary to introduce co-solvents in order to reach therapeutic concentrations of dissolved curcumin (Bagheri et al., 2020). Curcumin also degrades extensively at physiological conditions (pH 7.4) with a half-life of 20 min (Griesser et al., 2011). Therefore, numerous nanocarriers such as liposome, solid nanoparticles, polymeric micelles, metallic nanoparticle and quantum dots have been extensively studied to improve the solubility, stability, pharmacokinetics and bioavailability of curcumin (Karthikeyan et al., 2020).

Cumulative evidence suggests curcumin displays hormetic behavior in a dose-dependent manner (Moustapha et al., 2015; Rainey et al., 2015). Curcumin at low concentrations behaved as antioxidant agent to activate adaptive stress responses (Moustapha et al., 2015; Rainey et al., 2015). Conversely, at high concentrations, curcumin initiated a series of cytotoxic events leading to stress and eventual cell death. Several findings have demonstrated that curcumin could alleviate lung inflammation, histopathological injury and inflammatory cytokine expression *in vivo* (Wang et al., 2021; Xu and Liu, 2017; Yuan et al., 2022; Zhang et al., 2015). A Fe-curcumin based nanoparticles (Fe-Cur NPs) with dual functions effectively scavenged ROS in lung tissues and inflammation cytokine storm in mice with acute lung injury (ALI) following intravenous or intratracheal administration (Yuan et al., 2022). The reductions in macrophage cells, $CD3^{+}CD45^{+}$ T cells and inflammatory factors such as TNF-α, IL-1β, and IL-6 were more pronounced in mice receiving nanocurcumin compared to free drugs. This observation could be due to enhanced accumulation of nanocurcumin in lung tissues compared to free cucumin (Yuan et al., 2022).

Another study also showed similar findings whereby curcumin analog inhibited the inflammatory cell infiltration, cytokine levels in serum and broncho-alveolar lavage fluids (BALF) as well as pulmonary edema in rats (Zhang et al., 2015).

Our previous study showed that Cur-NPs attenuated the stress-induced inflammatory cytokines and protected alveolar macrophages from further damages (Lee et al., 2016). However, the cytotoxic responses of inactivated alveolar macrophages against Cur-NPs with different surface charges were not studied. Therefore, in this study, we challenged alveolar macrophages (NR8383) with escalating concentrations of Cur-NPs to measure the *in vitro* cytotoxic events. The elucidation of endocytic pathway internalization of Cur-NPs of different surface charges was determined to correlate the internalization rate and cytotoxicity of Cur-NPs. To investigate the above hypothesis, several toxicity-related assays were conducted which include the determination of intracellular ROS production, ATP content, membrane depolarization, lysosome oxidase, cytochrome c release, glutathione depletions, apoptosis and inflammation markers.

2. Materials and methods

2.1 Chemical and reagents

F12-K medium and fetal bovine serum were purchased from Invitrogen (Sydney, Australia). CellTiter 96 MTS reagent was supplied by Promega Co, USA. Annexin V-APC, 7AAD, Elisa kits for measurement of TNF-α and IL-6 were purchased from BD Biosciences (Sydney, Australia). Lipopolysaccharide (LPS), 3,3′,5,5′-tetramethylbenzidine (TMB), chlorpromazine (CPZ), colchicine (COL), cytochalasin B (Ctyo B), cytochalasin D (Cyto D), dynasore (DYN), methyl-beta-cyclodextrin (MβCD), nocodazole (NOC), U73122, wortmannin (WRT), polyinosinic acid

(PIA), dichlorofluorescin diacetate (DCFA) and mitochondrial membrane potential assay kit (MAK159) were obtained from Sigma (Sydney, Australia). Analytical grade absolute ethanol and acetonitrile were supplied from Fronine (Sydney, Australia). All chemicals and reagents were used without further purification.

2.2 Synthesis and characterization of Cur-NPs

The synthesis of Cur-NPs with different surface charges is performed based on protocols published previously (Lee et al., 2016). Different polymers at a concentrations of 0.3% w/w were used as to confer varying surface charges on the nanoparticles. They were polyvinyl alcohol (PVA), polyvinylpyrrolidone (PVP) and dextran. Void nanoparticles without curcumin (VP-NPs) coated with respective polymers were synthesized in the same manner (Chang et al., 2014; Chen et al., 2017; Lee et al., 2015; Lee et al., 2016).

The particle size distribution and zeta potential of Cur-NPs was measured using Malvern Zetasizer Nano ZS with the following settings: the refractive index for CUR was 1.41, the viscosity of water was 1.0002 mPas and temperature at 25 °C. Particle size and its distribution was determined immediately after preparation. For surface charge determination, 1 mg/mL of freeze-dried Cur-NPs was re-suspended in phosphate buffer saline (pH 7.4) and pH was maintained with either 0.1 N HCl or 0.1 M NaOH. The drug loading is calculated using the following equation:

$$Drug\ loading = \frac{weight\ of\ drug\ in\ nanoparticles}{weight\ of\ nanoparticles}\ x\ 100\%$$

2.3 Cell culture and maintenance

Rat alveolar macrophage cells (NR8383) were purchased from American Type Culture Collection (ATCC) and maintained according to ATCC recommendation. These mixtures of adherent and

floating cells were grown in F12-K medium with heat-inactivated fetal bovine serum (10% v/v) and incubated in humidified chamber supplied with 5% CO_2 at 37°C. The cells in the culture flask were gently scrapped and transferred into centrifuged tube together with the floating cells before centrifuged at 1000 rpm for 5 min. The cell culture medium was changed for every 2 to 3 days (Lee et al., 2016).

2.4 Cell toxicity assays

2.4.1 MTS assay

Prior to the cell toxicity evaluation, approximately 100 µL of medium containing 5×10^4 cells were seeded into a single well of 96 well plates and incubated overnight in the humidifier chamber with 5% CO_2 at 37°C. This was followed by 100 µL of Cur-NPs treatment at different concentrations (0–1000 µg/mL) for 3 days. To measure the cytotoxicity effect, 20 µL of MTS reagent was added into each well and incubated for 4 h before measuring the absorbance at 490 nm using a microplate reader (POLARstar, BMG Labtech, Germany). The cell viability was determined by comparing the absorbance Cur-NP treated cells to the untreated cells (control). Each concentration was performed in triplicate (Lee et al., 2016).

2.4.2 Reactive Oxygen Species (ROS) measurement

Intracellular ROS levels were measured using dichlorodihydrofluorescein diacetate (DCFH-DA). NR8383 cells (5×10^4 cells/well) were seeded in 96 well plates and incubated for 12 h before treated with Cur-NPs at different concentrations (0–1000 µg/mL) for 24 h. After Cur-NPs treatment, cells were centrifuged at 1000 rpm for 5 min and replaced with HBSS medium (100 µL) with 5 µM DCFH-DA in HBSS for 18 h at 37°C in dark condition. A cell free-supernatant

(100 µL) was transferred into 96 well plates before measuring the fluorescence intensity at 485 nm (excitation) and 535 nm (emission) using SpectraMax M2 (Molecular devices, Sydney, Australia). In this experiment, ascorbic acid (1 mM) and hydrogen peroxide (0.03%) were used as negative and positive controls, respectively. At least three independent experiments were conducted (Lee et al., 2020).

2.4.3 Mitochondrial membrane potential (MMP)

The effect of Cur-NP with different surface charges in modulating MMP of alveolar macrophage were measured with JC-10 MMP assay kit (MAK159) as previously described (Lee et al., 2020). Prior to the treatment, briefly, 5×10^4 cells per well were established into a black 96-well plate and incubated for overnight. Up to 1000 µg/mL of different Cur-NP were added to the prepared cells and incubated for another 24 h. The 96 well plate was centrifuged at 1000 rpm for 5 min to remove the culture medium and residual Cur-NP and washed twice with pre-warmed PBS before stained with JC-10 dye based on supplier protocol. The intensity of green (λ_{ex}= 490/ λ_{em} = 525 nm) and red fluorescence (λ_{ex}= 540/ λ_{em}= 590 nm) of the samples were measured using SpectraMax M2 (Molecular devices, Sydney, Australia). The percentage of MMP depletion was determined by calculating the ratio between red and green fluorescence intensity. Three independent experiments were conducted for each tested concentration.

2.4.4 Adenosine triphosphate (ATP) production

The ATP levels in NR8383 after treatment with different concentrations (0–1000 µg/mL) of Cur-NPs were measured using luminescent ATP detection assay kit (Abcam, Sydney, Australia) as previously described (Lee et al., 2020). For this, 5×10^4 cells per well were inoculated into 96-well

plates containing phenol-free F12-K complete medium and incubated overnight at 37°C. Then, the 96-well plates were centrifuged at 1000 rpm for 5 min and the supernatant were carefully removed from the wells. Next, 100 µL of medium containing Cur-NPs at different concentration were added into each well and incubated for another 6 h. Further procedures were conducted according to the protocol provided by manufacturer prior to the measurement of luminescence density (FLUOstar® Omega, BMG LABTECH, Ortenberg, Germany). Three independent experiments were conducted for this experiment.

2.4.5 Lysosomal isolation and oxidase activity determination of entrapped curcumin nanoparticles

Isolation of lysosomes from NR8383 cells were conducted according to published methods (Asati et al., 2010). Briefly, 5×10^5 of cells were seeded onto 35 mm petri dishes and incubated at 37°C for 12 h followed by treatment with Cur-NPs at different concentrations (0–1000 µg/mL) for 24 h. The cells were harvested and washed with PBS, then re-suspended in 1 mL of isotonic sucrose solution which consisted of $CaCl_2$ (8.8 g/L), sucrose (85.5 g/L) and Tris HCl (1.5 g/L) to lyse the cells into cytosolic and organelles. The lysate was centrifuged at 25,000 *g* for 15 min and followed with re-suspension of pellet in 1 mL of solution containing KCl (11.2 g/L) and 1.5 g/L Tris-HCl and centrifuged at 25,000 *g* for 15 min to sediment the lysosomes. The lysosome was further treated overnight with 200 µL of TMB at 1 mg/mL at room temperature. The reaction of lysosome with TMB was measured by absorbance at 652 nm using a microplate reader (POLARstar, BMG Labtech, Germany).

2.4.6 Cell apoptosis

The effect of Cur-NPs in inducing apoptosis on NR8383 was studied using 7-amino-actinomycin D (7-AAD) and Annexin V-APC staining protocols based on the manufacturer's instructions (BD Biosciences, Australia). For this purpose, approximately, 1×10^6 cells were seeded onto 35 mm petri dishes and incubated for 12 h before treated with Cur-NPs at different concentrations (0–50 µg/mL). After 24 h of treatment, the cells were gently detached from the petri dishes by scrapping, followed with PBS washing to remove the excess Cur-NPs and medium. The cell pellet was suspended in 100 µL of binding buffer (1×) and followed with 5 µL of 7-AAD and 5 µL of Annexin V-APC with incubation for 20 min in dark condition. Then, the cell suspensions were analyzed for apoptotic populations using Accuri™ C6 flow cytometry (BD Biosciences, Sydney, Australia) with at least 10000 events. The experiments were conducted in triplicate independently.

2.4.7 Caspase-3 measurement

The production of caspase-3 in alveolar macrophage challenged with Cur-NPs of different surface charge (0–50 µg/mL) was measured using caspase-3 assay kit (Abcam, Sydney, Australia). Briefly, 1×10^6 cells were seeded onto the 96-well plates, incubated overnight and treated with Cur-NPs for 24 h. Prior to the measurement, the NPs-free cells were collected by centrifugation and subjected to cell lysis procedures as per protocol by manufacturer. The samples were standardized to the protein concentration of 100 µg/50 µL before proceeding to further assay protocols. The fluorescence intensity of the samples was taken after 2 h at 400 nm (excitation) and 505 nm (emission) using SpectraMax M2 (Molecular devices, Sydney, Australia). Caspase-3 level is expressed as ratio of sample intensity to untreated control intensity.

2.4.8 Cytochrome C measurement

Prior the cytochrome C measurement, NR8383 cells (1×10^6 cells) were grown in 96-well plate for 24 h. After incubation with different Cur-NPs (0–50 μg/mL) for 24 h, the cells were centrifuged at 2000 *g* at 4 °C for 10 min. Cell pellet was mixed with cell lysis buffer and adjusted to 100 μg/mL of total protein and assayed according to the protocols provided by manufacturer (Abcam, Sydney, Australia). The absorbance of final reactant was measured using microplate reader at 550 nm and the cytochrome C concentration was expressed in ng/mL (POLARstar, BMG Labtech, Germany).

2.4.9 Glutathione measurement

The glutathione content in NR8383 after treated with Cur-NPs (0–50 μg/mL) for 24 h was measured using glutathione assay kit (Abcam, Sydney, Australia). Nanoparticle-free pellet was lysed and centrifuged at 13000 *g* for 20 min in refrigerated condition. The supernatant was further reacted with reagents provided by manufacturer and the fluorescence intensity was measured at λ_{ex}/ λ_{em}=380/460 nm using a SpectraMax M2. The glutathione concentration was expressed in ng/million cells.

2.4.10 Western Blot analysis

NR8383 grown on 6-well culture plates were lysed in RIPA buffer (Thermo Fisher Scientific, Waltham, MA) with protease inhibitor cocktail (Thermo Fisher Scientific, Waltham, MA, USA). The supernatants from each sample were collected to measure Bax and Bcl-2 expressions using Western blots performed as previously described (Chen et al., 2014). After transferred to polyvinylidene difluoride membrane (PVDF-Immobilon-P, Millipore, MA, USA), samples were blotted with specific primary antibodies overnight at 4 °C. Primary antibodies and dilutions are as

follows: Bax (1:1000) and Bcl-2 (1:1000), β-actin (1:1000) (Abcam, Cambridge, UK). Protein bands were detected using HRP-conjugated secondary antibody followed by chemiluminescence detection and imaged with Kodak Image Station Camera 4000 MM (Eastman Kodak Co., New York, NY, USA). The amount of protein present in each sample was determined as the densitometric density.

2.5 Induction of release of inflammation markers from alveolar macrophages

NR8383 at density of 5×10^5 cells were seeded onto the 6 well plate and grown for 24 h. Different concentrations of Cur-NPs were added to the pre-incubated cells. At different time point, cells-free medium was collected by centrifugation at 2000 *g* at 4 °C for 10 min and aliquots were stored at –80 °C until further use. LPS at 10 ng/mL was added to the cells as a positive control, meanwhile cells without Cur-NPs treatment were treated as negative control. Cytokines such as TNF-α and IL-6 was measured using ELISA kit (BD Biosciences, Sydney, Australia) according to the manufacturer's instructions.

2.6 Intracellular uptake of curcumin nanoparticles into alveolar macrophages

Approximately 5×10^6 cells/well were seeded onto 6 well plate before been treated with different inhibitors. All inhibitors were solubilized in dimethyl sulfoxide (DMSO) and the concentration used for the inhibition study was based on the viability of NR8383 (above 90% of cell viable). Cells were pretreated with inhibitors at specific final concentrations (chlorpromazine: 20 μM, colchicine: 10 μM, cytochalasin B: 10 μM, cytochalasin D: 10 μM, dynasore: 5 μM, methyl-beta-cyclodextrin: 5 μM, nocodazole: 30 μM, U6756: 10 μM, wortmannin: 2.5 μM and Polyinosinic acid: 10 μM) for 2 h before treated with Cur-NPs at (10 μM) for another 2 h. Subsequently, cells

were harvested and washed with PBS (3x) before analyzed by flow cytometry with at least 10000 events counted. Cells with and without Cur-NPs only were set as positive and negative control, respectively (Lee et al., 2019).

2.7 Statistical analysis

Each experiment was conducted in triplicate and data are expressed as mean ± standard error of mean (SEM). Analysis of data is done using two-way analysis of variance (ANOVA). The statistical significance of data is determined by Tukey test. A p value of < 0.05 is considered statistically significant.

3. Results

3.1 Surface-charge dependent toxicities

This study attempted to evaluate the toxicological events which occurs in alveolar macrophage as a response to NPs internalizations of different surface charge. The characterization of Cur-NPs in terms of particle size (using both DLS and transmission electron microscope), polydispersity index and encapsulation efficiency with different surface charges has been documented in our previous study (Lee et al., 2016). Briefly, the surface charges of fabricated nanoparticles ranged from –20.1 mV to +5.5 mV, depending on the type of polymer with the mean particle size of 30 nm (Supplementary Figure 1). PVP coating was responsible for the positive surface charges of Cur-NPs. Meanwhile, PVA and dextran coatings resulted in negative and neutral surface charges, respectively. The drug loading for positively charged Cur-NPs, negatively charged Cur-NPs and neutral Cur-NPs is 10.5 ± 0.3%, 9.9 ± 0.7% and 9.7 ± 0.8%. The cytotoxic effects of Cur-NPs with different surface charges against alveolar macrophages were measured using MTS assay as shown

in Figure 1a. It should be noted that the concentrations used in the MTS assays refer to the curcumin concentration present in each nanoparticle formulation. This means that the amount of Cur-NPs with different surface charges for MTS assay has been normalized to ensure that the concentration for all nanoparticle formulation is the same. In general, the overall cell viability was reduced with increasing concentration of curcumin (up to 1000 µg/mL) irrespective of NPs surface charge. The cell viability was maintained above 80% when treated with 0.9 µg/mL Cur-NPs. The positively charged Cur-NPs (denoted as PVP coated Cur-NPs) exerted the strongest cytotoxic effect with the IC_{50} values at 9.77 ± 0.51 µg/mL followed by negatively charged Cur-NPs (19.33 ± 0.97 µg/mL) and neutral charged Cur-NPs being the least toxic with the IC_{50} values of 33.68 ± 1.23 µg/mL. In addition, void polymeric nanoparticles (with different surface charges) were also included in the cytotoxicity evaluation and the results confirmed that these polymers were non-toxic to the cells, as the viability was maintained above 90% (Supplementary Figure 2).

To further understand the cytotoxic effect of the Cur-NPs, the reduction of mitochondrial membrane potential (MMP) in NR8383 was measured. As shown in Figure 1b, all the tested formulations demonstrated toxicity effect in a concentration dependent manner, in agreement with MTS assay. Both neutral (denoted as dextran coated Cur-NPs) and negatively charged Cur-NPs (denoted as PVA coated Cur-NPs) were less cytotoxic compared to positively charged Cur-NPs, as the MMP levels were maintained at 90% when treated with 1 µg/mL. However, the changes in MMP level in NR8383 was more sensitive towards positively charged Cur-NPs even at lower concentration (0.24 µg/mL). More than 80% of reduction in MMP was observed when NR8383 were treated with 1000 µg/mL of positively charged Cur-NPs. Meanwhile, no significant differences were noted between neutral and negatively charged Cur-NPs in the reduction of MMP

levels. The MMP levels when treated with 1000 µg/mL of neutral and negative Cur-NPs were maintained at 31 ± 3.6% and 36 ± 3.5%, respectively. In addition to MTS and MMP level measurement, the toxicity of the formulations towards NR8383 were further evaluated for ATP production (Figure 1d). Our results demonstrated that the ATP production of in NR8383 presented the following rank order: neutral charge > negative charge > positive charge. The LD_{50} in the reduction of ATP production for positively charged Cur-NPs, negatively charged Cur-NPs and neutral Cur-NPs was 7.9 µg/mL, 45.8 µg/mL and 85.7 µg/mL, respectively. In general, all the formulations demonstrated concentration-dependent toxicities on the production of ATP in NR8383.

Excessive production of ROS is associated with the cellular toxicity. Consequently, the level of ROS generated by NR8383 when challenged with different concentration of Cur-NPs were investigated (Figure 1c). It was found that lower concentrations of curcumin did not contribute to the increase in intracellular ROS production. The level of ROS in NR8383 was normal (denoted as 100%) to NR8383 exposed to Cur-NPs (5 µg/mL) exposure irrespective of surface charges. When exposed to 15.6 µg/mL of Cur-NPs, one-fold increase in intracellular ROS level for NR8383 was noted for positively charged Cur-NPs. Meanwhile, no increase in ROS level was observed for both negative and neutral surface charged Cur-NPs at the same concentration. Up to 6-fold increase of ROS level was noted for positive surface charged Cur-NPs when cells were exposed to high Cur concentration (1000 µg/mL). This was followed with 3-fold increase and two-fold increase in ROS level for cells treated with negative and neutral surface charged Cur-NPs (Figure 1c). Therefore, the intracellular ROS production results agreed with the cytotoxicity profile as measured in MTS assay.

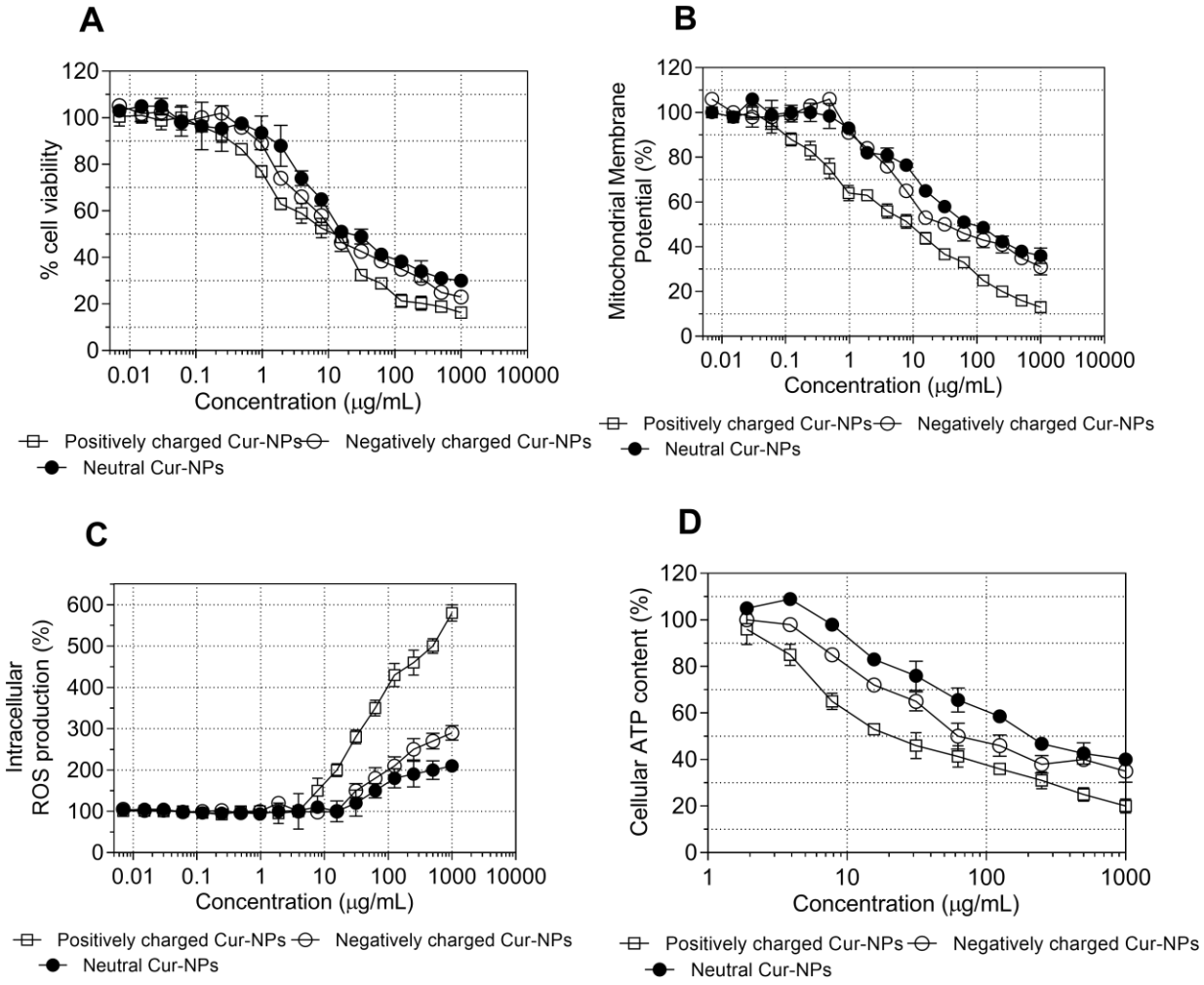

Figure 1. The effect of different surface charges of Cur-NPs on a) cell viability, c) mitochondrial membrane potential, c) intracellular ROS production and d) ATP content of NR8383 cells. Data are expressed as mean ± SEM of three replicates. *Concentration at x-axis for graphs refers to the exact concentration of Cur present in nanoparticle formulation.

The oxidase-like activity of Cur-NPs in acidic condition was measured to assess the localization of NPs in the lysosome via TMB oxidation (Figure 2a). Our results showed that positive Cur-NPs induced the highest lysosome oxidization activity in NR8383, regardless of the different

concentrations (10–1000 µg/mL) tested. The results also corroborated with other toxicity experiments whereby negatively charged NPs (OD value: 0.58 ± 0.03) was less potent in terms of inducing lysosome oxidization compared to positively charged NPs (OD value: 0.89 ± 0.03) when challenged with respective concentration of curcumin (1000 µg/mL). The oxidase activity of positively charged Cur-NPs were statistically higher compared to the other two formulations at higher concentrations (100 to 1000 µg/mL) (Figure 2a).

As shown in figure 2b, the intracellular concentration of glutathione was depleted as the concentration of Cur-NPs was increased. Figure 2b showed that the glutathione activity gradually decreased from 147.0 ± 10.7 ng/million cells to 72.0 ± 6.7 ng/million cells when alveolar macrophages were exposed to 50 µg/mL of positive Cur-NPs The potency of positive Cur-NPs was statistically different compared to the activity of negative (92.0 ± 6.7 ng/million cells) and neutral (112.0 ± 6.7 ng/million cells) Cur-NPs. However, it should be noted that low concentration of Cur (10 µg/mL) were not statistically significant in glutathione activity among the three different Cur-NPs (Figure 2b). We measured the release of cytochrome C as an indirect indicator of Cur-NPs toxicity towards alveolar macrophages. As shown in Figure 2c, the release of cytochrome C was dependent of the surface charge on the NPs. In other word, the effect is also dependent on the type of polymers used as coating for Cur-NPs as the positive Cur-NPs resulted in the highest cytochrome C followed by negative and neutral Cur-NPs. For instance, when cells were challenged with 50 µg/mL of the formulations, cytochrome C expression followed a decreasing rank order: 39.8 ± 2.7 ng/mL (positive Cur-NPs) > 32.7 ± 1.3 ng/mL (negative Cur-NPs) > 25.0 ± 0.9 ng/mL (neutral Cur-NPs) (Figure 2c).

Prior to apoptosis measurement, we evaluated the caspase-3 expression in NR8383 grown in different concentration and charge of Cur-NPs (Figure 2d). Generally, the expressions of caspase-3 increased in a dose-dependent manner and directly correlated to the toxicity effect of formulations (Figure 2d). No statistical differences in caspase-3 activity among all formulations at low concentrations (5-10 μg/mL) were observed. Compared to the untreated control, approximately 2-fold increase in caspase-3 activity was observed in positive Cur-NPs (40 μg/mL). Meanwhile, 1.6-fold and 1.45-fold increase in caspase-3 activity was noted for negative Cur-NPs and neutral Cur-NPs, respectively. To further confirm the toxicity effect of surface charges of NPs on NR8383 cells, the populations of apoptotic cells stained with combination of Annexin V-APC and 7AAD were measured. Results demonstrated that the induction of apoptosis were surface charge related and concentration dependent. From Figure 2e, it showed that the positive Cur-NPs remained the most toxic formulation as the level of apoptotic cells was the highest among all formulations. The apoptotic populations of NR8383 were 66.8 ± 2.5 %, 52.0 ± 6.5 % and 39 ± 2.4 % when challenged with 50 μg/mL positively charged Cur-NPs, negatively charged Cur-NPs and neutral Cur-NPs, respectively (Figure 2e). We also investigated both control and Cur-NPs treated cells for the expression of Bax (apoptotic) and Bcl-2 (anti-apoptotic) using Western blot (Figure 2f). NR8383 challenged with Cur-NPs irrespective of the surface charges, showed induction in the expression of Bax compared to control. The proteins band demonstrated the highest density for positively charged Cur-NPs followed by negatively and neutrally charged Cur-NPs. As analyzed using densitometric approach, an increase relative to internal control by 3.6-fold, 3.4-fold and 2.5-fold of Bax protein was observed for positive and neutral Cur-NPs, respectively. On the other hand, the expressions of anti-apoptotic Bcl-2 protein was attenuated in the presence of Cur-NPs.

399 A magnitude of 3-fold decrease in Bcl-2 expression was observed for positively charged Cur-NPs
400 (Figure 2f).
401
402 Based on Figure 3a and 3b, at low concentrations (0–10 μg/mL), all three Cur-NPs did not promote
403 the expressions of cytokines (IL-6 and TNF-α) in NR8383. Generally, the presence of positive
404 Cur-NPs resulted in the highest expressions of IL-6 and TNF-α, followed by negative and neutral
405 Cur-NPs ($p < 0.05$). For instance, the IL-6 expressions in NR8383 in the presence of 1000 μg/ml
406 positive, negative and neutral Cur-NPs, were 1340 ± 78 pg/mL, 857 ± 65 pg/mL and 431 ± 60
407 pg/mL, respectively ($p < 0.05$) (Figure 3b). From the surface charge perspective, more than 2-fold
408 and 4-fold lower TNF-α expressions was noted in negative and neutral Cur-NPs, respectively as
409 compared to positively charged formulation (Figure 3a). In our previous study, we investigated
410 the anti-inflammatory effect of Cur-NPs with different surface charges against LPS-induced
411 NR8383 (Lee et al., 2016). The efficacy of Cur-NPs to reduce the cytokine expressions (IL-1β, IL-
412 6 and TNF-α) followed the decreasing trend: positive Cur-NPs > negative Cur-NPs > neutral Cur-
413 NPs (Lee et al., 2016).
414

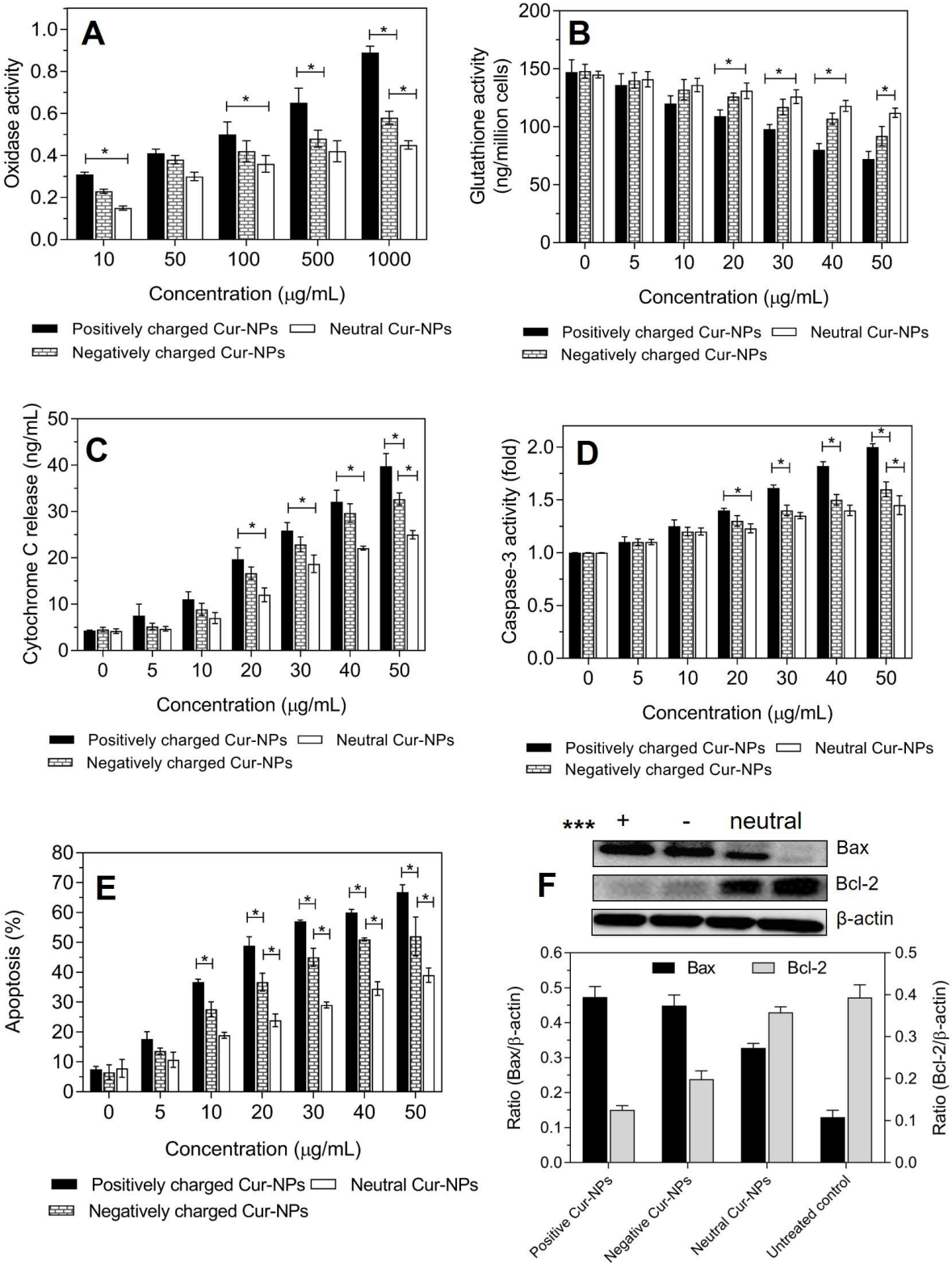
A
Oxidase activity
Concentration (μg/mL)
B
Glutathione activity (ng/million cells)
Concentration (μg/mL)
C
Cytochrome C release (ng/mL)
Concentration (μg/mL)
D
Caspase-3 activity (fold)
Concentration (μg/mL)
E
Apoptosis (%)
Concentration (μg/mL)
Positively charged Cur-NPs
Neutral Cur-NPs
Negatively charged Cur-NPs
F
*** + - neutral
Bax
Bcl-2
β-actin
Ratio (Bax/β-actin)
Ratio (Bcl-2/β-actin)
Positive Cur-NPs
Negative Cur-NPs
Neutral Cur-NPs
Untreated control

415

Figure 2. a) Oxidase-like activity, b) glutathione activity, c) cytochrome C release, d) caspase-3 and e) apoptotic populations in NR8383 cells when treated with varying concentrations of Cur-NPs of different surface charge. f) Western blot data showing the effects of different surface charge of Cur-NPs on the induction of apoptosis markers. NR8383 were treated with Cur-NPs for 24 h. After performing standard culture protocols of NR838 cells, western blot analysis was conducted to measure the Bax and Bcl-2 expressions. β-actin was used as an internal control. Data are expressed as mean ± SEM of three replicates. The bar graphs represent quantitative results obtained by densitometry analysis. *Significantly different at $p < 0.05$ (Tukey post hoc test). *** + refers to positively charged Cur-NPs; - refers to negatively charged Cur-NPs; neutral refers to neutral Cur-NPs. *Concentration at x-axis for graphs refers to the exact concentration of Cur present in nanoparticle formulation.

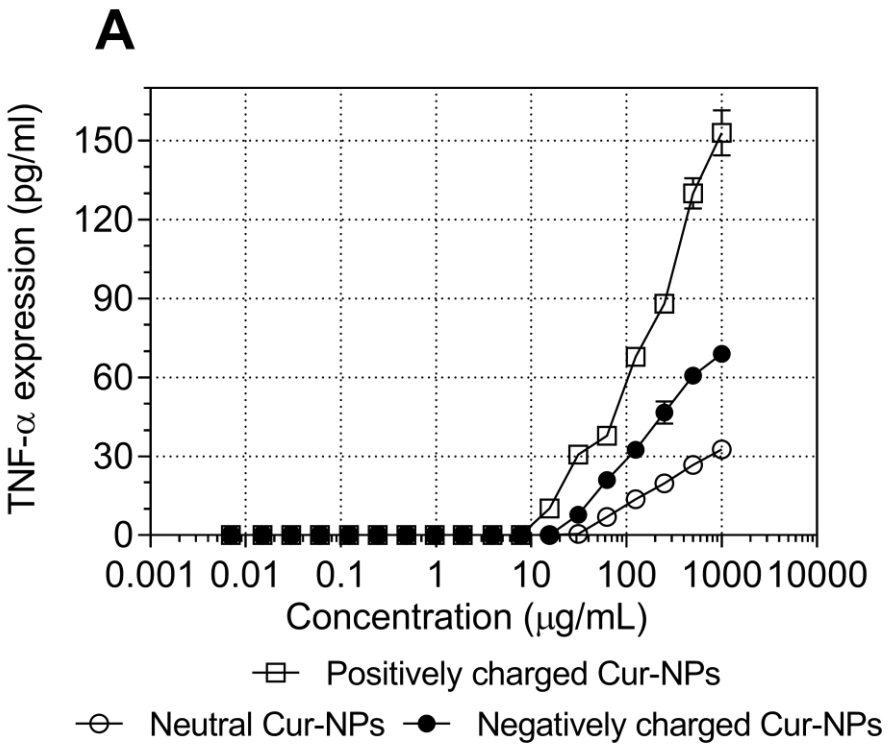
A
TNF-α expression (pg/ml)
150
120
90
60
30
0
0.001 0.01 0.1 1 10 100 1000 10000
Concentration (μg/mL)
Positively charged Cur-NPs
Neutral Cur-NPs
Negatively charged Cur-NPs

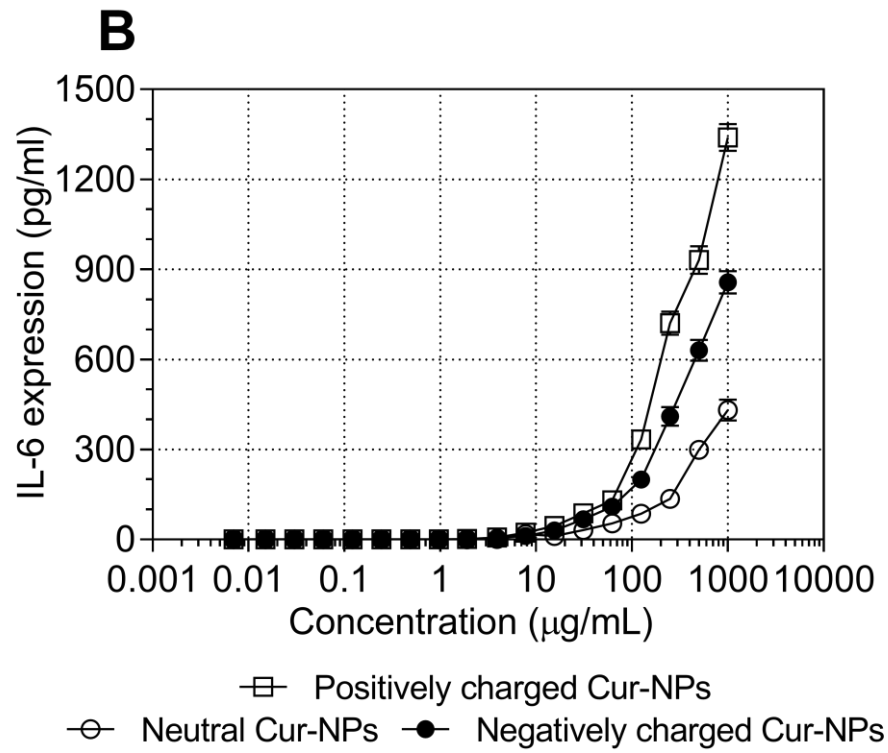
B
IL-6 expression (pg/ml)
1500
1200
900
600
300
0
0.001 0.01 0.1 1 10 100 1000 10000
Concentration (μg/mL)
Positively charged Cur-NPs
Neutral Cur-NPs
Negatively charged Cur-NPs

428

Figure 3. The effect of surface charge on nanoparticle on the induction of inflammation in NR8383. a) TNFα expressions and b) IL-6 expressions. Data are expressed as mean ± SEM of three replicates. *Concentration at x-axis for graphs refers to the exact concentration of Cur present in nanoparticle formulation.

3.2 Surface-charge dependent internalization of Cur-NPs

Based on the flow cytometry analysis, NR8383 had the highest uptake of positive Cur-NPs followed by negative and neutral Cur-NPs (Figure 4a). This observation led us to investigate the cellular receptors involved in the internalization of Cur-NPs. Different pathway inhibitors were used for studying the mechanism uptake pathway, including MβCD, CPZ, COL, WRT, DYN, NOC, PIA, Cyto B and Cyto D (Figure 4b-d). Based on Figure 4b, the cellular uptake of positive Cur-NPs was significantly affected in the presence of clathrin-mediated endocytosis such as Cyto B and DYN. The internalization of Cur-NPs for Cyto B and DYN was 25.6 ± 3.5% and 28.1 ± 4.3, respectively (Figure 4b). In addition, the presence of COL which acts to disrupt the microtubule (MT) polymerization also resulted in significant inhibition of cellular uptake whereby only 34.1 ± 6.0 % Cur-NPs was internalized. Particle internalization was also affected in the presence of NOC which caused MT disassembly. Cyto D which is an inhibitor of phagocytosis also contributed to 60% inhibition in cellular uptake of positive Cur-NPs. Meanwhile, other inhibitors exerted moderate inhibitory effect in which the cellular internalization of Cur-NPs, in the range of 65 to 75% (Figure 4b). Therefore, it is evident that the internalization of positively charged Cur-NPs is predominantly driven by clathrin-mediated endocytosis and phagocytosis with MT polymerization. Negatively charged Cur-NPs also demonstrated similar particle internalization behavior as positively charged Cur-NPs as shown in Figure 4c. Similarly, COL, DYN, NOC and

Cyto D inhibitors demonstrated the highest inhibition in particle internalization into NR8383 cells. Approximately, 40.3 ± 6.0%, 35.2 ± 1.9%, 43.6 ± 5.5% and 40.1 ± 3.3% NPs entered alveolar macrophage cells for COL, DYN, NOC and Cyto D, respectively (Figure 4c). On the other hand, the predominant cellular uptake pathway of neutral Cur-NPs appeared to rely on phagocytosis, since the pretreatment with Cyto D reduced the uptake to 26.1 ± 2.8%. Other inhibitors such as COL, PIA, DYN, MβCD and CPZ resulted in higher cellular uptake (up to 60%) (Figure 4d).

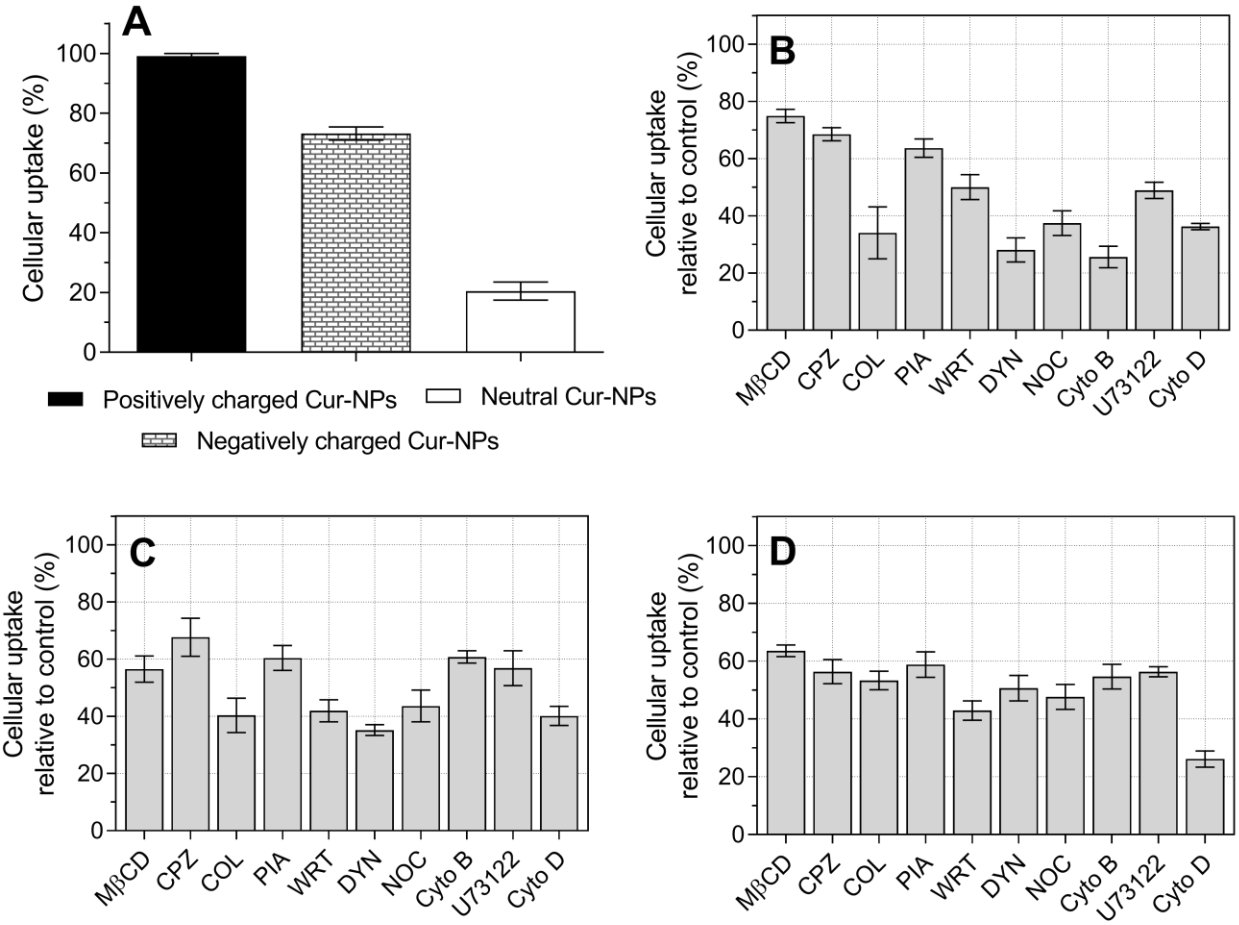

Figure 4. a) The efficacy of internalization of nanoparticles of varying surface charges into NR8383 cells as normalized against control (100%). Inhibition of cellular internalization of b) Positively charged Cur-NPs, c) Negatively charged Cur-NPs and d) Neutral Cur-NPs in the

presence of either endocytosis or phagocytosis inhibitors. Data are expressed as mean ± SEM of three replicates and measured using flow cytometry. *Significantly different at $p < 0.05$ (Tukey post hoc test).

MβCD, methyl-beta-cyclodextrin; CPZ, chlorpromazine; COL, colchicine; PIA, polyinosinic acid; WRT, wortmannin; DYN, dynasore; NOC, nocodazole; Cyto B, cytochalasin B; Cyto D, cytochalasin D

4. Discussion

Curcumin is widely known for its antioxidant, anti-inflammatory, anti-cancer and antibacterial properties (Lee et al., 2013). The log P value of curcumin at neutral pH is 3.0, making it a hydrophobic molecule with poor solubility in physiological media, resulting in poor bioavailability (Priyadarsini, 2014). Various approaches were undertaken to resolve the solubility issue including encapsulation of curcumin into nanocarriers (Karthikeyan et al., 2020). Curcumin is also a hormetic agent where it confers protective effect at low doses whereas at high doses, it activates acute response such as ROS stress, pro-inflammation and cell death. For instance, curcumin is an antioxidant at low concentrations but switches into pro-oxidant mode at concentrations >20 µM and causes depletion in intracellular glutathione levels (Rainey et al., 2015). We have shown that Cur-NPs could act as anti-inflammatory and pro-inflammatory agent in controlled experimental conditions. As shown in Figure 3, Cur-NPs did not induce any cytokine expressions at low concentrations. At higher concentrations however, the induction of inflammatory cytokine was charge dependent with the following decreasing trend: positive Cur-NPs > negative Cur-NPs > neutral Cur-NPs. In our previous study, we have demonstrated that positively charged Cur-NPs showed the highest anti-inflammatory activities against LPS-induced alveolar macrophages. This

was followed with negatively charged Cur-NPs and finally neutral Cur-NPs (Lee et al., 2016). The anti-inflammatory activities of Cur-NPs is believed to be associated with the NF-κB inhibition that suppressed cytokine expression (Zhong et al., 2011). In addition, it is known that oxidative stress enhanced lung airway inflammation via stress kinases and redox-sensitive transcription factors (Rahman and Adcock, 2006). We found a correlation in which the anti-inflammatory actions were stronger in Cur-NPs with higher anti-oxidant activities in our previous study, thus demonstrating a possible synergistic link between anti-oxidant activity of curcumin to its innate anti-inflammatory effect (Lee et al., 2016).

Many studies have established that curcumin possesses selective toxicity towards targeted areas while exerting negligible effects against healthy cells (Chang et al., 2014; Chen et al., 2017; Lee et al., 2015). At low concentrations, curcumin provided protective effects towards hepatocytes cell through reduction of lipid peroxidation and cytochrome C release (Ghoneim, 2009). However, high concentrations caused a reversal of activity whereby activation of apoptotic associated proteins (i.e., caspase-3) coupled with glutathione reduction was observed (Ghoneim, 2009). The viability of cells after exposure to NPs were found to be dependent to the surface charges of the NPs in this study. Positively charged Cur-NPs exerted higher inhibitory effect in the cell survival compared to neutral and negatively charged Cur-NPs. Similar observations were also noted whereby triblock copolymers functionalized with positively charged compounds such as ammonia, N,N-dimethylethanolamine or pyridine were more toxic against NR8383 cells compared to carboxylic acid functionalized triblock copolymers (Bhattacharjee et al., 2013). In a separate study, cationic silicon NPs demonstrated the highest toxicity effect (EC_{50}: 12 ng/mL) in NR8383 cells

compared to nonionic silicon NPs (EC_{50}: 270 ng/mL). Surprisingly, anionic silicon NPs did not possess toxicity effect across the tested concentrations (3000 ng/mL) (Bhattacharjee et al., 2010).

Glutathione plays an important role to regulate cell viability through interchangeable intracellular levels of ROS. The presence of thiol group in its cysteine moiety endows the antioxidant activity in glutathione which could be reversibly oxidized (McBean, 2017). Curcumin is widely regarded as an excellent antioxidant, presumably due to its capability to donate electron/proton to reactive oxygen species from *o*-methoxyphenol group. However, many have demonstrated the curcumin switches from antioxidant to pro-oxidant behavior in a dose-dependent manner (Moustapha et al., 2015; Rainey et al., 2015). Lower concentrations of curcumin reduced lipid peroxidation and cytochrome *c* release while glutathione depletion, caspase activation and ROS induction were provoked at higher concentrations. Impaired antioxidant defense mechanisms in cells are an indirect result of conjugation between curcumin to thiols groups causing the glutathione depletion. Our results demonstrated that positively charged Cur-NPs were the most potent in reducing glutathione level in NR8383 cells, leading to the higher toxicity of curcumin owing to higher intracellular bioavailability. In addition, the highest intracellular ROS levels in NR8383 after incubated with positive Cur-NPs further supported the pro-oxidant activity of curcumin. Syng-ai and coworkers reported a more than 50% reduction of glutathione in MCF-7 and MDAMB cells after treatment with curcumin (50 µmol/L) (Syng-Ai et al., 2004). Interestingly no reduction in glutathione was observed in normal hepatocyte cells. This observation is in accord with our results, whereby the depletion of glutathione in NR8383 is associated with cytotoxicity of Cur-NPs. We further speculated that the higher internalization rate of Cur-NPS is the contributing factor towards

529 the depleted glutathione in cells as the pro-oxidant behavior of Cur-NPs is concentration-
530 dependent.
531
532 We next examined the internalization mechanisms of Cur-NPs with different surface charges into
533 alveolar macrophages. This is because the selective and toxicity actions of curcumin could be
534 associated with internalization and localization of this phenolic compound within cells. Previous
535 studies showed that surface charge is linked to the uptake pathway of NPs, whereby NPs with
536 cationic surface were predominantly internalized via clathrin-mediated endocytosis (Chakraborty
537 and Jana, 2015; Tan et al., 2010). In addition, NPs with surface charge of > +20 mV displayed
538 stronger interactions with cells, induced higher membrane damage and thus higher cell cytotoxicity
539 (Tan et al., 2010). The uptake of NPs with surface charge ranging from +10 mV to −10 mV
540 occurred via multiple pathways including clathrin-mediated endocytosis and lipid raft endocytosis
541 (Chakraborty and Jana, 2015). It should be noted that NPs internalization in our study was
542 measured at short incubation time, as the inhibition of one endocytic pathway results in activation
543 of other endocytic mechanisms (dos Santos et al., 2011). The optimal incubation time for
544 measuring internalization is also needed to allow sufficient time for detectable levels of NPs in
545 alveolar macrophages without severe cytotoxic effects incurred from the inhibitors. We have tested
546 ten different inhibitors for this study which blocked the major endocytic pathways such as clathrin-
547 mediated endocytosis (CPZ, DYN, Cyto B), lipid-raft mediated endocytosis (MβCD), caveolae
548 mediated endocytosis (MβCD) and phagocytosis (Cyto D). DYN was used to determine whether
549 the entry of Cur-NPs is dynamin-dependent. COL and NOC inhibition of uptake show that
550 internalization was MT-dependent. Meanwhile, PIA is a specific inhibitor of entry via mannose
551 receptor and U73122 inhibits the kinase/phospholipase regulated pathway. Results showed that

552 the uptake of positive and negative Cur-NPs is significantly blocked by the clathrin-mediated
553 endocytosis and phagocytosis. Disruption of MT polymerization and assembly also contributed to
554 the reduced intake of Cur-NPs (Figure 5).
555
556 Our results are in agreement with earlier reports where non-PEGylated cationic quantum dots were
557 uptaken into cells predominantly via clathrin-mediated endocytosis (Chithrani and Chan, 2007).
558 Rapid internalization of positively charged NPs could be due to the favorable ionic interactions
559 with cell membrane which facilitated cell entry via clathrin pits (Chakraborty and Jana, 2015; Tan
560 et al., 2010). However surface chemistry could alter the endocytic uptake pathway of NPs as
561 functionalization of octyl onto non-PEGylated cationic quantum dots shifted the uptake pathway
562 from clathrin-mediated endocytosis to lipid raft-mediated endocytosis (Chakraborty and Jana,
563 2015). Our study also showed that the cytoskeleton (microtubules, actin and dynamin) was
564 essential in the uptake of positively charged Cur-NPs into alveolar macrophages.
565
566 On the other hand, the involvement of multiple endocytic pathways such as phagocytosis, clathrin-
567 mediated endocytosis and micropinocytosis indicated the non-specificity of neutral Cur-NPs,
568 which corroborated findings by Charkraborty and Jana (Chakraborty and Jana, 2015). In contrast,
569 recent findings showed that irrespective of the nanocarrier (i.e., different composition,
570 hydrophobicity and particle size) used, the internalization of NPs occurred mainly via caveolae-
571 mediated endocytosis and macropinocytosis (Yan et al., 2019). Most polymeric NPs which enter
572 into cells predominantly via clathrin-mediated endocytosis are trafficked to acidic
573 endosomal/lysosomes compartment to be degraded. Our previous study demonstrated that Cur-
574 NPs with average size of 30 nm were localized in perinuclear region and cell cytoplasm in various

cancer cell and healthy cell lines (Lee et al., 2015). The targeting of curcumin to subcellular organelles suggested that the NPs used in our study were able to escape the endosomal/lysosome intact. Furthermore, it is believed that curcumin targets the lysosome to induce lysosomal destabilization and autophagy (Moustapha et al., 2015; Sala de Oyanguren et al., 2020).

In line with the previous study, our data showed the accumulation of Cur-NPs in alveolar macrophages exerted oxidation of lysosome with positively charged NPs exhibiting the highest activity. Curcumin is known to bind directly to the transcription factor EB, TFEB (master regulator of autophagy and lysosomal biogenesis) (Zhang et al., 2016) via α,β-unsaturated, carbonyl and enolic groups of the β-diketone moiety (Priyadarsini, 2014) and cause its delocalization from lysosome. Taken together, it is probable that positively charged Cur-NPs internalized via clathrin-mediated endocytosis were trafficked to the lysosome, caused oxidation and resulted in lysosomal stress and destabilization. It should be noted that positive Cur-NPs were capable to escape the lysosomal compartment as evident from the changes in MMP, glutathione and ROS levels which are linked to mitochondrial destabilization (Figure 1b, 1c and 2b). As reported by Nagahama et al, the curcumin compound that was encapsulated in NPs became protonated at endosomal acidic pH condition (Nagahama et al., 2016). This caused the influx of Cl^- ion and water molecules leading to increased osmotic pressure in lysosomal membrane. Subsequently, possible disruption of membrane might occur and thus enabling the escape of Cur-NPs from endosome/lysosome to the cytoplasm. (Nagahama et al., 2016; Shrestha et al., 2012).

On the other hand, for neutral Cur-NPs that entered into cells via micropinocytosis, clathrin-mediated endocytosis and phagocytosis, predominant lysosome trafficking of NPs is still expected

as the kinetic of clathrin-mediated endocytosis is relatively faster compared to other endocytic pathways (Chakraborty and Jana, 2015). However, neutral Cur-NPs that successfully bypassed lysosome localization could be trafficked directly to other subcellular organelles such as nucleus; thus explaining the weaker oxidation of lysosome observed in figure 2a. Many studies have noted that amphiphilic NPs (<50 nm) designed for lipid raft/caveolae-mediated endocytosis accumulate in the nucleus (Mazumdar et al., 2021; Zhou et al., 2014). Ruan et al demonstrated that TAT peptide functionalized NPs entered cells through micropinocytosis and localized in the nucleus (Ruan et al., 2007).

Although we observed a significant reduction in MMP and ATP levels in NR8383 following the exposure to Cur-NPs, previous publications indicated no direct interactions between curcumin and mitochondrial membrane. The authors demonstrated that curcumin was not accumulated inside the mitochondria but was instead localized around it (Chakraborty and Jana, 2015; Moustapha et al., 2015). Furthermore, curcumin induced mitochondrial swelling via a calcium-dependent mechanism, which is intimately linked to endoplasmic reticulum-stress-associated calcium release. The released calcium ion was taken up by mitochondria to cause mitochondrial swelling and finally lead to cytochrome C release and caspase activation (Moustapha et al., 2015). We therefore hypothesized in our study that the destabilization of mitochondria is largely due to the calcium release from endoplasmic reticulum which entered mitochondria, changed electron transport chain and consequently resulted in MMP, ATP reduction and increased ROS generation (Figure 1 and 2). Our study also noted high population of apoptotic cells and increase in Bax/Bcl-2 ratio following Cur-NPs exposure. Cell apoptosis is interconnected with mitochondrial

destabilization as permeable mitochondria induced the activation of caspases and pro-apoptotic proteins including Bax and cytochrome *c*.

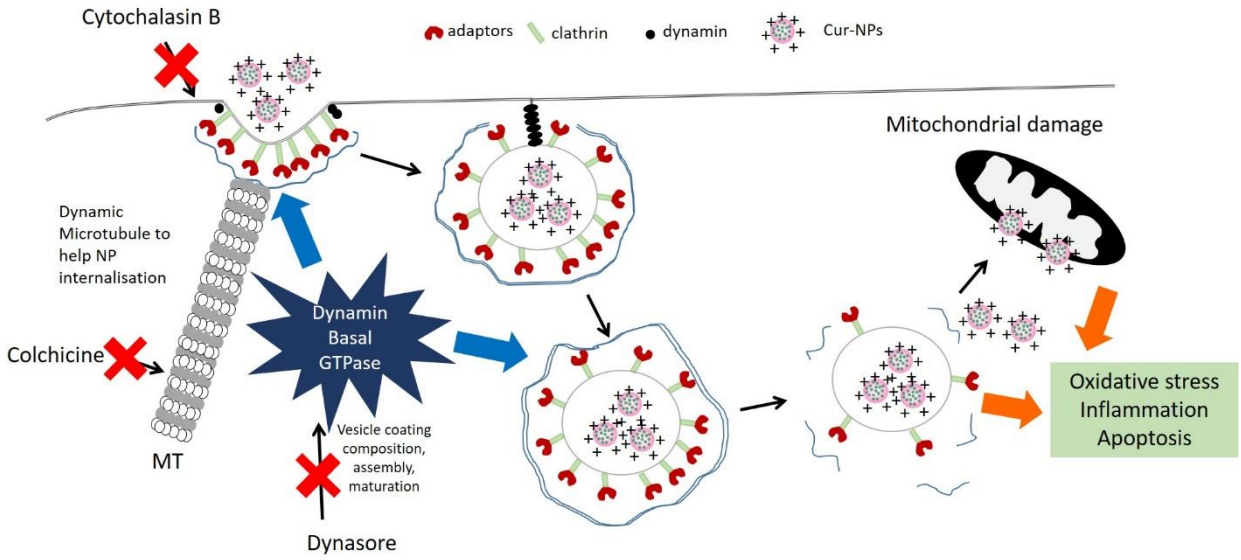

Figure 5. Schematic representation of the proposed internalization, localization and toxicity mechanisms of positively charged Cur-NPs in alveolar macrophages.

Based on our data, the cytotoxicity of Cur-NPs towards alveolar macrophages is surface-charge dependent which in turn is associated to the uptake pathway and localization of Cur-NPs in cells. Overall, we demonstrate that positively charged Cur-NPs mediates the cytotoxicity of alveolar macrophages through lysosomal and mitochondrial-associated destabilization via entry through clathrin-mediated endocytosis (Figure 5). Nanoparticle internalization occurred predominantly via clathrin-mediated endocytosis with stability of MT and actin, playing an important rule to facilitate entry. Upon entry into NR8383, Cur-NPs were trafficked into endosome/lysosome and caused extensive lysosomal stress and oxidation. Subsequently, Cur-NPs were released from the

endosome/lysosome, inducing mitochondrial destabilization, cytochrome c release and ROS production followed by caspase activation and mitochondrial-associated apoptosis. As the surface charge of NPs were near to neutral, clathrin-mediated endocytosis is no longer the predominant internalization route and NPs could enter the cells via other endocytic pathways. As a result, the oxidative-induced lysosomal stress and subsequent cytotoxicity effect against alveolar macrophages were significantly reduced.

5. Conclusions

This study provides evidence that a surface-charge dependent cytotoxicity of Cur-NPs in NR8383 that is associated with the uptake of the NPs. Positively charged Cur-NPs were the most cytotoxic towards NR8383, followed by negatively charged and neutral Cur-NPs. The positively charged Cur-NPs exerted its cytotoxicity through the lysosomal and mitochondrial destabilization. The trafficking of Cur-NPs upon entry via clathrin-mediated endocytosis caused lysosomal stress and eventual release of NPs into cytosol, thus resulting in loss of MMP, glutathione depletion, cytochrome c release, ROS production and apoptosis.

6. Acknowledgements

The authors thank the Ministry of Higher Education (MOHE) Malaysia for the financial support provided via the Fundamental Research Grant Scheme (FRGS/1/2018/STG03/UNIKL/02/2).

7. Declaration of competing interest

There are no conflicts of interest.

8. Credit authorship contribution statement

Ching-Yee Loo: Conceptualization, formal analysis, investigation, writing – Original Draft. **Ee Ling Siew**: Writing – Review & Editing. **Paul M. Young**: Resources, writing – Review & Editing. **Daniela Traini**: supervision, writing – Review & Editing. **Wing-Hin Lee**: Conceptualization, methodology, investigation, funding acquisition, writing – Review & Editing.

9. References

2005. Chapter 10 Fate of deposited particles, in: C.-s. Wang (Ed.), Interface Science and Technology. Elsevier, pp. 149-158.

Abdel-Diam, M.M., Samak, D.H., El-Sayed, Y.S., Aleya, L., Alarifi, S., Alkahtani, S., 2019. Curcumin and quercetin synergistically attenuate subacute diazinon-induced inflammation and oxidative neurohepatic damage, and acetylcholinesterase inhibition in albino rats. Environmental science and pollution research international 26, 3659-3665.

Aggarwal, V., Tuli, H.S., Varol, A., Thakral, F., Yerer, M.B., Sak, K., Varol, M., Jain, A., Khan, M.A., Sethi, G., 2019. Role of Reactive Oxygen Species in Cancer Progression: Molecular Mechanisms and Recent Advancements. Biomolecules 9.

Asati, A., Santra, S., Kaittanis, C., Perez, J.M., 2010. Surface-Charge-Dependent Cell Localization and Cytotoxicity of Cerium Oxide Nanoparticles. ACS Nano 4, 5321-5331.

Bagheri, H., Ghasemi, F., Barreto, G.E., Rafiee, R., Sathyapalan, T., Sahebkar, A., 2020. Effects of curcumin on mitochondria in neurodegenerative diseases. BioFactors 46, 5-20.

Bhattacharjee, S., de Haan, L.H.J., Evers, N.M., Jiang, X., Marcelis, A.T.M., Zuilhof, H., Rietjens, I.M.C.M., Alink, G.M., 2010. Role of surface charge and oxidative stress in cytotoxicity of organic

monolayer-coated silicon nanoparticles towards macrophage NR8383 cells. Particle and Fibre Toxicology 7, 25.

Bhattacharjee, S., Ershov, D., Gucht, J.v.d., Alink, G.M., Rietjens, I.M.C.M., Zuilhof, H., Marcelis, A.T.M., 2013. Surface charge-specific cytotoxicity and cellular uptake of tri-block copolymer nanoparticles. Nanotoxicology 7, 71-84.

Chakraborty, A., Jana, N.R., 2015. Clathrin to Lipid Raft-Endocytosis via Controlled Surface Chemistry and Efficient Perinuclear Targeting of Nanoparticle. The Journal of Physical Chemistry Letters 6, 3688-3697.

Chang, R., Sun, L., Webster, T.J., 2014. Short communication: selective cytotoxicity of curcumin on osteosarcoma cells compared to healthy osteoblasts. International journal of nanomedicine 9, 461-465.

Chen, L., Ge, Q., Tjin, G., Alkhouri, H., Deng, L., Brandsma, C.-A., Adcock, I., Timens, W., Postma, D., Burgess, J.K., Black, J.L., Oliver, B.G.G., 2014. Effects of cigarette smoke extract on human airway smooth muscle cells in COPD. European Respiratory Journal 44, 634.

Chen, W., Li, L., Zhang, X., Liang, Y., Pu, Z., Wang, L., Mo, J., 2017. Curcumin: a calixarene derivative micelle potentiates anti-breast cancer stem cells effects in xenografted, triple-negative breast cancer mouse models. Drug Deliv 24, 1470-1481.

Chithrani, B.D., Chan, W.C.W., 2007. Elucidating the Mechanism of Cellular Uptake and Removal of Protein-Coated Gold Nanoparticles of Different Sizes and Shapes. Nano Letters 7, 1542-1550.

Doello, K., Ortiz, R., Alvarez, P.J., Melguizo, C., Cabeza, L., Prados, J., 2018. Latest in Vitro and in Vivo Assay, Clinical Trials and Patents in Cancer Treatment using Curcumin: A Literature Review. Nutrition and Cancer 70, 569-578.

dos Santos, T., Varela, J., Lynch, I., Salvati, A., Dawson, K.A., 2011. Effects of Transport Inhibitors on the Cellular Uptake of Carboxylated Polystyrene Nanoparticles in Different Cell Lines. PLOS ONE 6, e24438.

Ghoneim, A.I., 2009. Effects of curcumin on ethanol-induced hepatocyte necrosis and apoptosis: implication of lipid peroxidation and cytochrome c. Naunyn-Schmiedeberg's archives of pharmacology 379, 47-60.

Griesser, M., Pistis, V., Suzuki, T., Tejera, N., Pratt, D.A., Schneider, C., 2011. Autoxidative and cyclooxygenase-2 catalyzed transformation of the dietary chemopreventive agent curcumin. J Biol Chem 286, 1114-1124.

Karthikeyan, A., Senthil, N., Min, T., 2020. Nanocurcumin: A Promising Candidate for Therapeutic Applications. Frontiers in Pharmacology 11.

Laskin, D.L., Malaviya, R., Laskin, J.D., 2019. Role of Macrophages in Acute Lung Injury and Chronic Fibrosis Induced by Pulmonary Toxicants. Toxicological sciences : an official journal of the Society of Toxicology 168, 287-301.

Lee, W.H., Bebawy, M., Loo, C.Y., Luk, F., Mason, R.S., Rohanizadeh, R., 2015. Fabrication of Curcumin Micellar Nanoparticles with Enhanced Anti-Cancer Activity. J Biomed Nanotechnol 11, 1093-1105.

Lee, W.H., Loo, C.Y., Bebawy, M., Luk, F., Mason, R.S., Rohanizadeh, R., 2013. Curcumin and its derivatives: their application in neuropharmacology and neuroscience in the 21st century. Curr Neuropharmacol 11, 338-378.

Lee, W.H., Loo, C.Y., Rohanizadeh, R., 2019. Functionalizing the surface of hydroxyapatite drug carrier with carboxylic acid groups to modulate the loading and release of curcumin nanoparticles. Mater Sci Eng C Mater Biol Appl 99, 929-939.

727 Lee, W.H., Loo, C.Y., Traini, D., Young, P.M., 2020. Development and Evaluation of Paclitaxel
728 and Curcumin Dry Powder for Inhalation Lung Cancer Treatment. Pharmaceutics 13.
729 Lee, W.H., Loo, C.Y., Young, P.M., Rohanizadeh, R., Traini, D., 2016. Curcumin Nanoparticles
730 Attenuate Production of Pro-inflammatory Markers in Lipopolysaccharide-Induced Macrophages.
731 Pharm Res 33, 315-327.
732 Lugg, S.T., Scott, A., Parekh, D., Naidu, B., Thickett, D.R., 2021. Cigarette smoke exposure and
733 alveolar macrophages: mechanisms for lung disease. Thorax, thoraxjnl-2020-216296.
734 Mazumdar, S., Chitkara, D., Mittal, A., 2021. Exploration and insights into the cellular
735 internalization and intracellular fate of amphiphilic polymeric nanocarriers. Acta pharmaceutica
736 Sinica. B 11, 903-924.
737 McBean, G.J., 2017. Cysteine, Glutathione, and Thiol Redox Balance in Astrocytes. Antioxidants
738 6.
739 Moustapha, A., Pérétout, P.A., Rainey, N.E., Sureau, F., Geze, M., Petit, J.M., Dewailly, E.,
740 Slomianny, C., Petit, P.X., 2015. Curcumin induces crosstalk between autophagy and apoptosis
741 mediated by calcium release from the endoplasmic reticulum, lysosomal destabilization and
742 mitochondrial events. Cell Death Discovery 1, 15017.
743 Murthy, S., Larson-Casey, J.L., Ryan, A.J., He, C., Kobzik, L., Carter, A.B., 2015. Alternative
744 activation of macrophages and pulmonary fibrosis are modulated by scavenger receptor,
745 macrophage receptor with collagenous structure. FASEB journal : official publication of the
746 Federation of American Societies for Experimental Biology 29, 3527-3536.
747 Nagahama, K., Utsumi, T., Kumano, T., Maekawa, S., Oyama, N., Kawakami, J., 2016. Discovery
748 of a new function of curcumin which enhances its anticancer therapeutic potency. Scientific
749 Reports 6, 30962.

Priyadarsini, K.I., 2014. The Chemistry of Curcumin: From Extraction to Therapeutic Agent. Molecules 19.

Rahman, I., Adcock, I.M., 2006. Oxidative stress and redox regulation of lung inflammation in COPD. Eur. Respir. J. 28, 219-242.

Rainey, N., Motte, L., Aggarwal, B.B., Petit, P.X., 2015. Curcumin hormesis mediates a cross-talk between autophagy and cell death. Cell Death & Disease 6, e2003-e2003.

Ruan, G., Agrawal, A., Marcus, A.I., Nie, S., 2007. Imaging and Tracking of Tat Peptide-Conjugated Quantum Dots in Living Cells: New Insights into Nanoparticle Uptake, Intracellular Transport, and Vesicle Shedding. Journal of the American Chemical Society 129, 14759-14766.

Sala de Oyanguren, F.J., Rainey, N.E., Moustapha, A., Saric, A., Sureau, F., O'Connor, J.-E., Petit, P.X., 2020. Highlighting Curcumin-Induced Crosstalk between Autophagy and Apoptosis as Supported by Its Specific Subcellular Localization. Cells 9.

Shrestha, R., Elsabahy, M., Florez-Malaver, S., Samarajeewa, S., Wooley, K.L., 2012. Endosomal escape and siRNA delivery with cationic shell crosslinked knedel-like nanoparticles with tunable buffering capacities. Biomaterials 33, 8557-8568.

Syng-Ai, C., Kumari, A.L., Khar, A., 2004. Effect of curcumin on normal and tumor cells: role of glutathione and bcl-2. Mol Cancer Ther 3, 1101-1108.

Tan, S.J., Jana, N.R., Gao, S., Patra, P.K., Ying, J.Y., 2010. Surface-Ligand-Dependent Cellular Interaction, Subcellular Localization, and Cytotoxicity of Polymer-Coated Quantum Dots. Chemistry of Materials 22, 2239-2247.

Wang, Y., Wang, Y., Cai, N., Xu, T., He, F., 2021. Anti-inflammatory effects of curcumin in acute lung injury: In vivo and in vitro experimental model studies. International Immunopharmacology 96, 107600.

773 Xu, Y., Liu, L., 2017. Curcumin alleviates macrophage activation and lung inflammation induced
774 by influenza virus infection through inhibiting the NF-κB signaling pathway. Influenza Other
775 Respir Viruses 11, 457-463.
776 Yan, X., Cao, S., Li, Y., Xiao, P., Huang, Z., Li, H., Ma, Y., 2019. Internalization and subcellular
777 transport mechanisms of different curcumin loaded nanocarriers across Caco-2 cell model. Journal
778 of Drug Delivery Science and Technology 52, 660-669.
779 Yuan, R., Li, Y., Han, S., Chen, X., Chen, J., He, J., Gao, H., Yang, Y., Yang, S., Yang, Y., 2022.
780 Fe-Curcumin Nanozyme-Mediated Reactive Oxygen Species Scavenging and Anti-Inflammation
781 for Acute Lung Injury. ACS Central Science 8, 10-21.
782 Zhang, J., Wang, J., Xu, J., Lu, Y., Jiang, J., Wang, L., Shen, H.M., Xia, D., 2016. Curcumin
783 targets the TFEB-lysosome pathway for induction of autophagy. Oncotarget 7, 75659-75671.
784 Zhang, Q., Lin, J.-L., Thomas, P.S., 2014. Reactive Oxygen Species and Obstructive Lung
785 Disease, in: I. Laher (Ed.), Systems Biology of Free Radicals and Antioxidants. Springer Berlin
786 Heidelberg, Berlin, Heidelberg, pp. 1643-1670.
787 Zhang, Y., Liang, D., Dong, L., Ge, X., Xu, F., Chen, W., Dai, Y., Li, H., Zou, P., Yang, S., Liang,
788 G., 2015. Anti-inflammatory effects of novel curcumin analogs in experimental acute lung injury.
789 Respiratory research 16, 43.
790 Zhong, F., Chen, H., Han, L., Jin, Y., Wang, W., 2011. Curcumin Attenuates Lipopolysaccharide-
791 Induced Renal Inflammation. Biol. Pharm. Bull. 34, 226-232.
792 Zhou, N., Zhu, S., Maharjan, S., Hao, Z., Song, Y., Zhao, X., Jiang, Y., Yang, B., Lu, L., 2014.
793 Elucidating the endocytosis, intracellular trafficking, and exocytosis of carbon dots in neural cells.
794 RSC Advances 4, 62086-62095.
795